

FRAGMENTATION CROSS SECTIONS OF ^{56}Fe AT 471 A MeV ON Al, C AND CH₂ TARGETS

LI-CHUN WANG^a, DONG-HAI ZHANG^{b†}, SHIWEI YAN^{a,c‡}, YAN-JING LI^a
JIN-XIA CHENG^a, JUN-SHENG LI^b, S. KODAIRA^d, N. YASUDA^d

^aCollege of Nuclear Science and Technology, Beijing Normal University
Beijing 100875, China

^bInstitute of Modern Physics, Shanxi Normal University
Linfen 041004, China

^cBeijing Radiation Center, Beijing 100875, China

^dFundamental Technology Center, National Institute of Radiological Sciences
4-9-1 Anagawa, Inage-ku, Chiba 263-8555, Japan

(Received February 10, 2012; revised version received May 22, 2012)

We have measured the fragmentation cross sections of ^{56}Fe on Al, C and CH₂ targets at 471 A MeV using CR-39 plastic nuclear track detector. Cross sections for H target are calculated based on the results of C and CH₂ targets. Here, we present the results of total charge changing cross sections and the partial cross sections for fragments with charge $Z_F \geq 5$. The total charge changing cross sections agree well with other previous experimental results at different energies and the theoretical prediction of Bradt–Peters semi-empirical formula, which are approximately independent of the beam energy but increase with the increase of the target mass. The partial cross sections show a significant enhancement for the fragments with even- Z nuclei, especially for the fragments with charge $10 \leq Z_F \leq 20$. For the collisions of ^{56}Fe on all targets reported in this paper, we firstly present the partial cross section results of the fragments with charge $5 \leq Z_F \leq 9$ using CR-39 detector. Finally, the partial cross sections is compared with the prediction of the improved quantum molecular dynamical model (ImQMD) and the GEMINI model, the production of charged projectile fragments can be well described by the models.

DOI:10.5506/APhysPolB.43.1769

PACS numbers: 25.70.-z, 25.70.Mn, 25.60.Dz, 29.40.Wk

[†] Corresponding author: zhangdh@dns.sxnu.edu.cn

[‡] Corresponding author: yansw@bnu.edu.cn

1. Introduction

Fragmentation cross sections for heavy ions on different targets are very important in many fields [1,2,3]. In astrophysics, in order to determine cosmic ray source composition, people are primarily interested in the changes in energy and composition experienced by cosmic ray nuclei during interstellar propagation [4]. In the energy range of $10^2 \sim 10^4$ MeV/nucleon, the cosmic radiation arriving at the orbit of earth has its highest intensity, and the nuclear component consists of $\sim 87\%$ hydrogen, $\sim 12\%$ helium and the rest 1% consists of heavier nuclei ranging from carbon to actinides [5]. Among the heavy component of the galactic cosmic rays (GCR), ^{56}Fe is the heaviest element that abundantly presents in late phase of stellar evolution. With the acceleration of iron to relativistic energies, the first direct measurement of the astrophysically interesting fragmentation of iron was made at the Bevalac, Lawrence-Berkeley National Laboratory in 1979 [6]. Subsequently, several large laboratories have begun to participate in the subject of heavy-ion fragmentation by using distinctive equipment, such as Super Proton Synchrotron (SPS) in CERN, Alternating Gradient Synchrotron (AGS) in Brookhaven National Laboratory, accelerator facilities in NASA Space Radiation Laboratory and Heavy Ion Medical Accelerator in Chiba (HIMAC). Most of these experiments have been simulated in several theory models, such as parametrization method [7,8,9,10], scaling algorithm [11,12], NUCFRG2 code [13] and different intranuclear cascade models combined with different de-excitation models. However, there remain considerable discrepancies not only between experimental result and model prediction but also among experiments themselves, which direct us to make a systematic investigation using the same beam on different targets. In addition, the mechanism of fragmentation reaction has not been fully understood. It is necessary to study plenty of fragmentation events induced by all kinds of projectile nuclei at various energies. For the fragmentation of ^{56}Fe , many results have been published at energies between several hundred A MeV and several A GeV [6,8,14,15,16,17,18,19,20,21,22,23,24]. Recently, two groups [25,26] investigated the fragmentation of ^{56}Fe on a hydrogen target at different energies and the fragmentation of ^{56}Fe target irradiated by proton with different energies, the experimental results were compared with the predictions of different theoretical models. It is found that the parametric formulas cannot well explain total experimental data of ^{56}Fe fragmentation at energies from $300 A$ MeV to $1500 A$ MeV, each parametric formula has its application range. From the comparison of experimental results with the predictions of different intranuclear cascade models combined with different de-excitation models, it is found that the GEMINI model [27] not only gives a rather precise account of all cross sections but also reproduces

the recoil velocities, the mean values and widths of the isotopic distributions measured in studied beam energies. From these results it is difficult to definitely identify the production mechanism of the intermediate and light mass fragments. In this paper, we report results on fragmentation cross sections of ^{56}Fe at 471 A MeV aiming at filling the gap in the profile of experimental cross sections of fragmentation productions.

We choose carbon (C), aluminum (Al) and polyethylene (CH₂) as targets to study the fragmentation of iron projectile. Carbon can provide a sample of a light target nucleus. Since aluminum is an important component of the material surrounding many kinds of particle detector in space and balloon experiments, a detailed knowledge of its cross section gives a better correction for the interactions of cosmic rays in the detector systems. Polyethylene is a composite target which was used to obtain the cross sections on a hydrogen target. The interactions between Fe with hydrogen are of astrophysical interest because hydrogen is the dominant component of the interstellar medium. From nuclear physics point of view, the cross sections on a hydrogen target can be compared with fragmentation resulting from proton bombardment on heavy targets.

The quantum molecular dynamical (QMD) model is a semi-classical microscopic dynamical model [28]. It has been used to study the multifragmentation process at intermediate energies in heavy-ion collision extensively. In this paper, we use the improved quantum molecular dynamical (ImQMD) model to simulate the production of the charged fragments, which greatly improves the fermion properties of nuclei, the momentum and density distribution of ground state nuclei. Detailed description of ImQMD can be found in Ref. [29]. Because the ImQMD cannot fully describe the de-excited process of prefragments after a collision, we combine with the GEMINI model [27] when the fragment formation is completed within a time scale about 125 fm/ c in ImQMD. The GEMINI is a statistical-model code which allowed light-particle evaporation, symmetric fission and all possible binary-decay modes.

2. Experimental details

The stacks made of CR-39 nuclear track detectors and different targets were exposed at HIMAC with beams of 471 A MeV Fe ions. Fig. 1 shows the sketch of the sandwiched targets and CR-39 detectors setup. The CR-39 sheets are placed in front, middle and back of targets. In this experiment, we only use the front and middle CR-39 sheets in data analysis. The area of each CR-39 sheet is about $50 \times 50 \text{ mm}^2$. The thickness of the CR-39 detector is about 700 μm so that fewer fragments which are produced in the detector material can be neglected. The targets must be thick enough so that a rea-

sonable number of interactions occurs, but not too thick, otherwise multiple interactions in the target will cause a trouble. The thickness of the target for Al, C and CH₂ is 3 mm, 5 mm and 10 mm, respectively. The exposures were performed at normal incidence with a density of 3000 ions/cm². After exposure, the CR-39 detectors were etched in 7M NaOH aqueous solution at temperature of 70°C for 15 hours. Thus the ions which cross the detectors can be observed at both sides of the sheet using HSP-1000 microscope system. The PitFit software allows us to extract some geometric information, such as the position coordinates, the major and minor axes and the area of each etched track. With these conditions, about 1.5×10^4 Fe tracks are traced from the first detector surface in the stack. The base area of a cone produced by an iron ion is around $1100 \mu\text{m}^2$, while the smallest base area corresponding to projectile fragment with charge of $Z = 5$ is about $100 \mu\text{m}^2$.

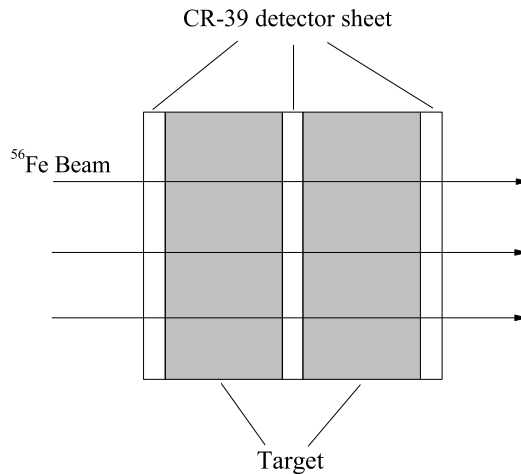


Fig. 1. Sketch of the target-detector configuration.

The number of projectile fragments leaving the targets is determined from the distribution of the etched base area. Fig. 2 shows the track base area distributions of Fe ions and their fragments (on the CH₂ target) in the CR-39 sheet. Peaks for Fe ion and each fragments with charge from $Z = 5$ to $Z = 25$ appear. The large one corresponds to the primary particles which comes out of the target without undergoing a nuclear interaction. According to the inherent charge resolution of the detector, we can identify the fragment charge down to $Z = 5$. A good linear relationship between the fragment charge and the etched cone area is shown in Fig. 3, which manifests a better resolution capability of the CR-39 detector and the reliability of the measurement accuracy of the experiment.

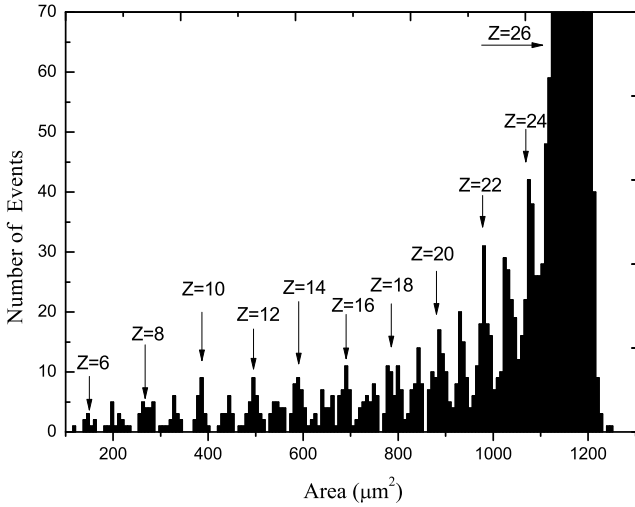


Fig. 2. Base area distribution of Fe ions and their fragments. The peak in the area $1130 \sim 1208 \mu\text{m}^2$ corresponds to Fe.

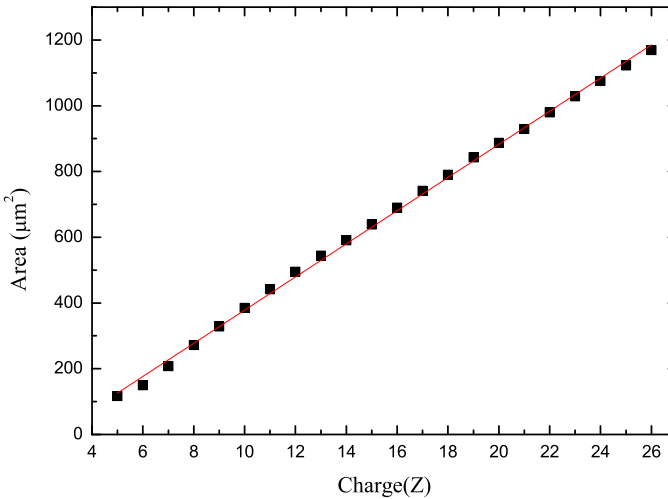


Fig. 3. Correlation between the projectile fragment charge and the mean etched fragment track area.

Here we use the tracking method which is mentioned in the reference [30]. Trajectories of ion tracks through the stack are reconstructed in two steps: (1) the track positions in CR-39 detector are corrected by parallel and rotational translations of coordinates (x and y) of tracks formed in the detectors. (2) the difference between the positions of corresponding tracks on the surfaces in the neighboring detector is minimized by a track matching routine.

The coordinates (x and y) of tracks formed in the detectors are translated because of the microscope scanning technology. The coordinates of tracks before the target (or front surface of CR-39 sheet) is (x and y) and of matching tracks after the target (or back surface of CR-39 sheet) is (x' and y'). Following the translation relation, the coordinate of matching track can be calculated as

$$x' = a_1x + b_1y + c_1, \quad (1)$$

$$y' = a_2x + b_2y + c_2, \quad (2)$$

parameters $a_1, b_1, c_1, a_2, b_2,$ and c_2 are determined using the least square methods. Then, we can obtain the corresponding coordinate ($x'_{\text{cal}}, y'_{\text{cal}}$) of (x, y). The difference $dx = x'_{\text{cal}} - x'$ and $dy = y'_{\text{cal}} - y'$ can help us to determine the matching track. Fig. 4 shows the track position differences on both sides of the detector and on the side in the front and back of the targets. If dx and dy are calculated for all combinations of positions for

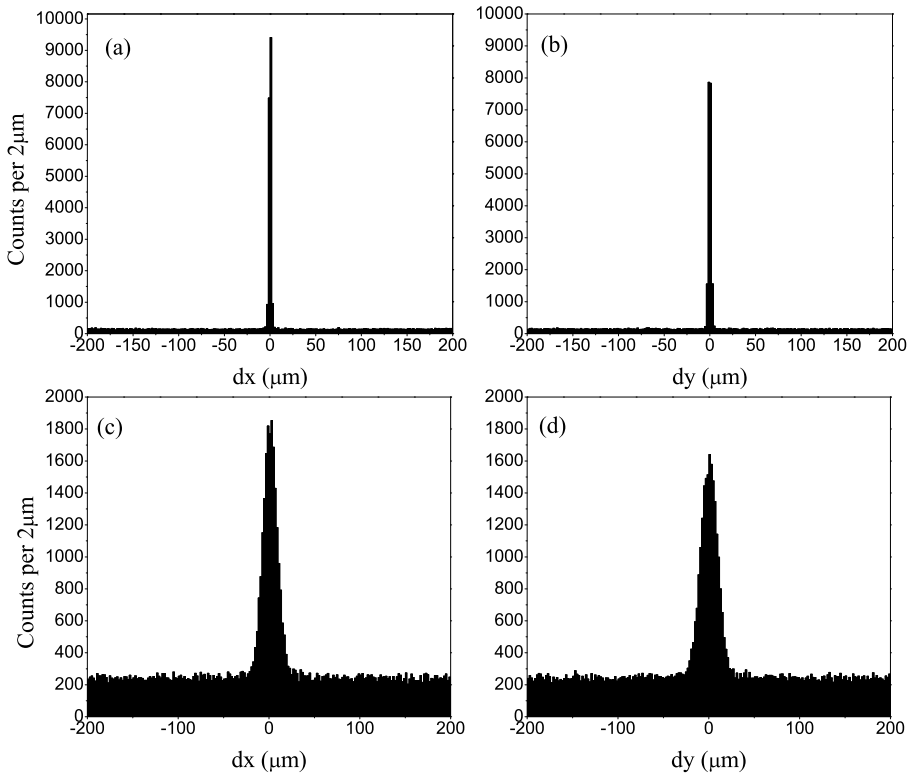


Fig. 4. Differences (dx and dy) for x and y given by subtraction of track coordinates on the other side. (a) and (b) show the differences between the sides of one detector, (c) and (d) show the differences between the sides before and after C target.

extracted tracks, only the correct combination ought to make a peak which appears in the figures, and the dx and dy values of other combination should be randomly distributed in the figures.

The deviations of the distributions of dx and dy (σ_x and σ_y) give position accuracies of tracks which are estimated to be 1.3–1.5 μm between the sides of one detector and 8–9 μm between the sides of the nearest neighboring targets. The accuracy suffers from Coulomb scattering with energy loss straggling and becomes significant on the downstream detectors.

The beam from the accelerator is not completely “clean” but contains a small fraction ($\leq 7\%$) of particles with different charges, presumably produced by interactions earlier in the beam path. In this case, we only select all of the iron tracks to trace from the first CR-39 sheet to the following CR-39 sheets, then the fragment tracks with different charges can be found on the detector after the target. There are several possibilities when matching tracks on the detector surfaces which are adjacent to the target.

- Within 4σ distance of x and y :
 1. There is no candidate track.

A completely fragmentation interaction occurred. The charge of the fragments are less than 5, which are so small that it cannot be identified by the detector.
 2. Only one candidate track is found.
 - (a) A trajectory formed in the detector without any nuclear reactions.
 - (b) A nuclear interaction occurred. The charge of the fragment is relatively large, near 25, but the emission angle is relatively small.
- Without 4σ distance of x and y , but within the limited fragmentation angle.
 1. There is one candidate track.

An elastic interaction occurred. The location after the target is changed more than 4σ , but the charge is not changed. This phenomenon is particularly obvious in CH_2 target.
 2. There are two or more candidate tracks are found.

One primary iron splits into two or three fragments with medium mass, and this accounts for a small fraction of all interaction events.

3. The total charge changing cross section

The total charge changing cross sections are determined with the survival fraction of ions using the following relation [17]

$$\sigma_{\text{tot}} = \frac{A_{\text{T}} \ln(N_{\text{in}}/N_{\text{out}})}{\rho t N_{\text{AV}}}, \quad (3)$$

where A_{T} is the nuclear mass of the target; N_{in} and N_{out} are the numbers of incident ions before and after the target, respectively. ρ [g/cm³] is the target density. t [cm] is the thickness of the target and N_{AV} is the Avogadro number.

Table I presents the total charge-changing cross sections for 471 A MeV Fe on H, C, CH₂ and Al targets. The cross section on hydrogen target is inferred from the results on C and CH₂ targets according to the relation [18]

$$\sigma_{\text{H}} = 0.5(\sigma_{\text{CH}_2} - \sigma_{\text{C}}). \quad (4)$$

TABLE I

The total charge changing cross sections for 471 A MeV Fe on different targets. Errors are statistical standard deviations.

Energy [A MeV]	Target	A_{T}	σ_{tot} [mb]
471	Al	27	1943 ± 106
471	C	12	1636 ± 44
471	CH ₂	4.7	2963 ± 70
471	H	1	664 ± 13

Fig. 5 shows our experimental results, the other experimental results [17, 18, 19, 20] and the predictions from Bradt–Peters semi-empirical formula [31] $\sigma_{\text{tot}} = \pi r_0^2 (A_{\text{P}}^{1/3} + A_{\text{T}}^{1/3} - b_0)^2$, where $r_0 = 1.35$ fm, $b_0 = 0.83$; A_{P} and A_{T} are the projectile and target mass number, respectively. For CH₂ target, the formula cannot be applied because it is a composite target. For H target, we choose $A_{\text{T}} = 0.089$ which is the same as that used by Westfall *et al.* [6] to calculate the total charge changing cross section. It is found that the results from Bradt–Peters formula agree well with our experimental results and others, the total charge changing cross sections are almost independent of beam energies. Fig. 6 shows the dependence of the total charge changing cross section on the target mass. Obviously, the total cross section increases as a function of target mass.

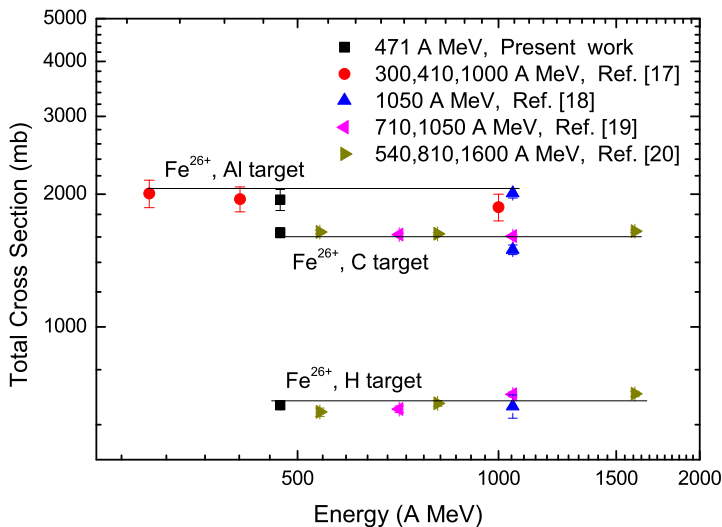


Fig. 5. Total charge changing cross sections for interactions of Fe on Al, C and H targets at different energies. Solid line represents the predictions from Bradt–Peters formula.

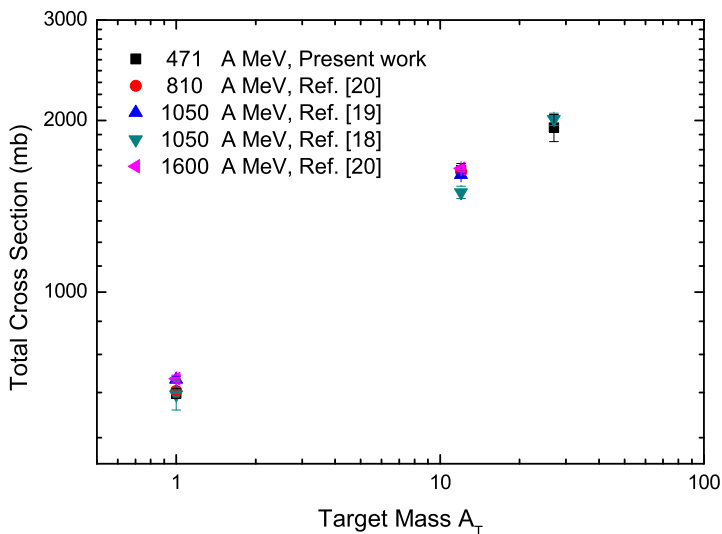


Fig. 6. Total charge-changing cross section of 471 A MeV Fe *versus* target mass number A_T .

4. The partial charge changing cross sections

The partial charge changing cross sections can be calculated using the following relation [17]

$$\sigma_{\Delta Z} = \frac{A_T}{\rho t N_{AV}} \left(\frac{N_{out}^f}{N_s^p} - \frac{N_{in}^f}{N_{in}^p} \right), \quad (5)$$

where N_{in}^f and N_{out}^f are the number of each fragment before and after the target, N_{in}^p and N_s^p are the numbers of incident and that of survived iron ions. In the present work, we only select all of the iron ions as the incident ones before the target, thus $N_{in}^f = 0$. In this case, the partial charge changing cross sections is changed into a simple relation

$$\sigma_{\Delta Z} = \frac{A_T}{\rho t N_{AV}} \frac{N_{out}^f}{N_s^p}. \quad (6)$$

In Fig. 7 and Table II, the partial cross sections of projectile fragment production are shown for interactions of Fe on Al, C, CH₂ and H targets at 471 A MeV. There is a sudden drop at $\Delta Z = 21$ ($Z_F = 5$) because of the detection limit of our detector.

For all targets, the fragment production cross section shows an obvious enhancement for even- Z nuclei, especially at $Z_F = 12$ and $Z_F = 14$. For the fragmentation of Fe on Al target, our experimental result agree well with the results from Ref. [18] at beam energy of 1050 A MeV and 1550 A MeV. For the fragmentation of Fe on C, CH₂ and H targets, our experimental results are generally consistent with other experimental ones [18,19,20,21,25], but it should be noticed that our experimental results are smaller than the results from Refs. [20,21] for fragments with charge $Z_F = 25, 24$ and greater than the results from Refs. [20,21] for fragment with charge $Z_F = 15$ ($\Delta Z = 11$) at nearly the same energy (540 A MeV). Because the base area of etched track for fragments with charge $Z_F = 25, 24$ is superposed with the base area of beam iron ions (as shown in Fig. 2), which results in some mistaken identification of fragment charge and some tracks of fragments with charge $Z_F = 25, 24$ is identified as beam tracks.

Fig. 8 shows the comparison between our experimental results and the simulations using ImQMD model and GEMINI model. We can find that the ImQMD just give an approximate estimate for the production of charged projectile fragments. After adding the GEMINI model, the odd-even effect can be observed evidently.

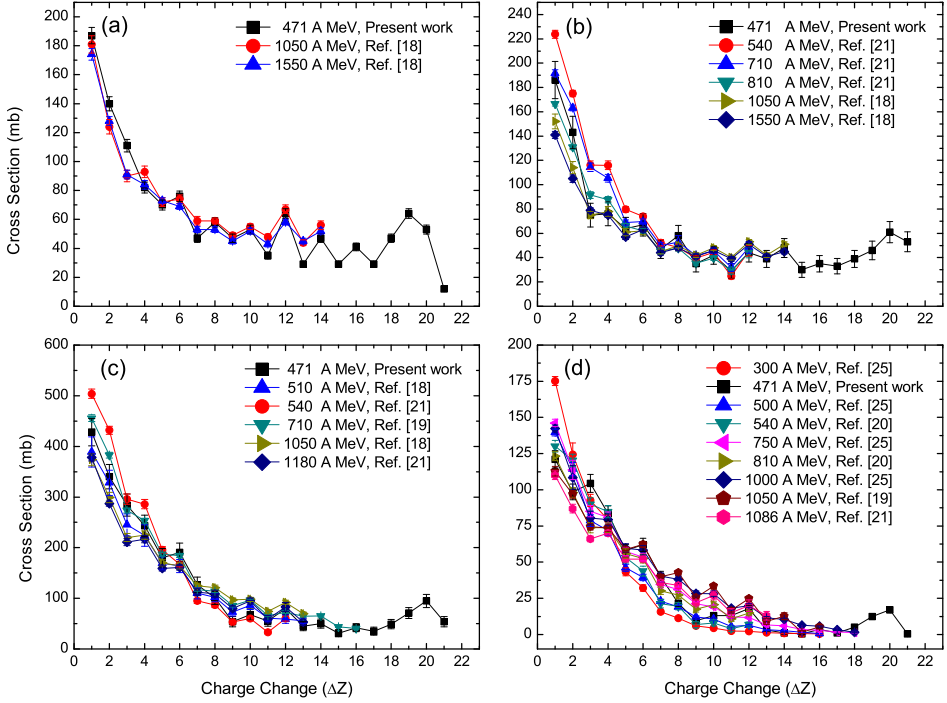


Fig. 7. Partial charge-changing cross sections for 471 A MeV Fe on Al (a), C (b), CH_2 (c) and H (d) targets, and the corresponding experimental results at different energies.

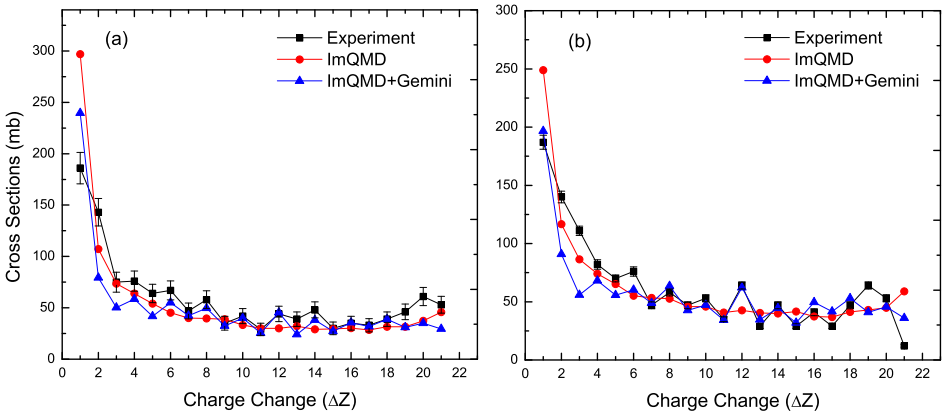


Fig. 8. Comparison of the partial cross sections for 471 A MeV Fe on C (a) and Al (b) target between experiment and simulation by using the ImQMD model added Gemini model.

TABLE II

The partial cross sections of fragment productions for 471 A MeV Fe on the Al, C, CH₂ and H targets.

ΔZ	σ [mb] Al target	σ [mb] C target	σ [mb] CH ₂ target	σ [mb] H target
1 ($Z_{\text{frag}} = 25$)	187 ± 6	186 ± 15.3	428 ± 27	121 ± 6.0
2 ($Z_{\text{frag}} = 24$)	140 ± 5	143 ± 13.4	340 ± 24	98.5 ± 5.4
3 ($Z_{\text{frag}} = 23$)	111 ± 4	75 ± 9.7	284 ± 22	104.5 ± 6.2
4 ($Z_{\text{frag}} = 22$)	82 ± 4	76 ± 9.8	243 ± 21	83.5 ± 5.3
5 ($Z_{\text{frag}} = 21$)	70 ± 3	64 ± 9	180 ± 18	58 ± 4.3
6 ($Z_{\text{frag}} = 20$)	76 ± 4	67 ± 9.2	191 ± 18	62 ± 4.5
7 ($Z_{\text{frag}} = 19$)	47 ± 3	47 ± 7.7	127 ± 15	40 ± 3.6
8 ($Z_{\text{frag}} = 18$)	58 ± 3	58 ± 8.6	101 ± 13	21.5 ± 2.3
9 ($Z_{\text{frag}} = 17$)	47 ± 3	35 ± 6.7	54 ± 10	9.5 ± 1.5
10 ($Z_{\text{frag}} = 16$)	53 ± 3	42 ± 7.3	68 ± 11	13 ± 1.8
11 ($Z_{\text{frag}} = 15$)	35 ± 2	29 ± 6.1	55 ± 10	13 ± 1.9
12 ($Z_{\text{frag}} = 14$)	64 ± 3	44 ± 7.5	80 ± 12	18 ± 2.1
13 ($Z_{\text{frag}} = 13$)	29 ± 2	39 ± 7	45 ± 9	3 ± 0.9
14 ($Z_{\text{frag}} = 12$)	47 ± 3	48 ± 7.8	50 ± 9	1 ± 0.8
15 ($Z_{\text{frag}} = 11$)	29 ± 2	30 ± 6.2	31 ± 7	0.5 ± 0.6
16 ($Z_{\text{frag}} = 10$)	41 ± 3	35 ± 6.7	42 ± 8	3.5 ± 0.9
17 ($Z_{\text{frag}} = 9$)	29 ± 2	33 ± 6.4	35 ± 8	1 ± 0.7
18 ($Z_{\text{frag}} = 8$)	47 ± 3	39 ± 7	49 ± 9	5 ± 1.1
19 ($Z_{\text{frag}} = 7$)	64 ± 3	46 ± 7.6	71 ± 11	12.5 ± 1.8
20 ($Z_{\text{frag}} = 6$)	53 ± 3	61 ± 8.8	95 ± 13	17 ± 2.0
21 ($Z_{\text{frag}} = 5$)	12 ± 1	53 ± 8.2	54 ± 10	0.5 ± 0.7

In order to characterize the odd–even effect, we adopt the quantity $V(Z_F)$ defined by Iancu *et al.* [32]

$$V(Z_F) = 2\sigma(Z_F)/[\sigma(Z_F + 1) + \sigma(Z_F - 1)], \quad (7)$$

where Z_F refers to the fragment species with charge Z . We combine the values of $V(Z_F)$ obtained for all odd- Z fragments into a single weighted average value, and similarly combine the results for all even- Z fragments to get that weighted average, and take the ratio of the two to obtain a single value for a given beam ion, energy and target. We find that the ratios for our experimental results are 1.65 ± 0.16 , 1.54 ± 0.43 , 1.54 ± 0.40 and 2.32 ± 0.89 for Al, C, CH₂ and H targets, respectively. It is obvious that the ratio for H target is more pronounced than that for Al, C and CH₂ targets. In the collisions of 471 A MeV ⁵⁶Fe and H target, almost no violent interaction take place, ⁵⁶Fe fragments into more stable nuclide, even- Z nuclide.

5. Conclusions

We have used CR-39 plastic nuclear track detectors to measure the total and partial charge changing cross sections for ^{56}Fe on Al, C and CH_2 at 471 A MeV. Comparing with other experimental results, it is found that the total charge changing cross section is independent of the beam energy and can be well described by the Bradt–Peters formula. The total cross section increases as a function of target mass number. The partial cross sections of projectile fragment productions are target dependent, and our results are generally in agreement with that from other experiments for the fragments with charge $10 \leq Z_F \leq 25$. There is a significant enhancement for even- Z nuclei especially in the range of $10 \leq Z_F \leq 20$. Finally, we firstly give the results of the partial charge changing cross section of the fragments with charge $5 \leq Z_F \leq 9$ using CR-39 detector. The ImQMD can be used to describe the production of the projectile fragments very well. Especially combing with the Gemini model, the odd–even effect can be observed evidently.

This work has been supported by the Chinese National Science Foundation under Grant Nos. 11075100 and 10975019, the Natural Science Foundation of Shanxi Province under Grant 2011011001-2, the Shanxi Provincial Foundation for Returned Overseas Chinese Scholars, China (Grant No. 2011-058), the Scientific Research Foundation for the Returned Overseas Chinese Scholars, Ministry of Personnel of China (Grant No. MOP2006138), and the Fundamental Research Funds for the Central Universities. We gratefully acknowledge the staff of the HIMAC for providing the beam to expose the stacks.

REFERENCES

- [1] P.L. Petti *et al.*, *Annu. Rev. Nucl. Part. Sci.* **44**, 155 (1994).
- [2] U. Amaldi, *Nucl. Phys.* **A751**, 409 (2005).
- [3] J.W. Wilson *et al.*, *Radiat. Environ. Biophys.* **34**, 217 (1995).
- [4] C.X. Chen *et al.*, *Phys. Rev.* **C49**, 3200 (1994).
- [5] J.A. Simpson, *Composition and Origin of Cosmic Rays*, edited by M.M. Shapiro, Reidel, Dordrecht 1983, p. 1.
- [6] G.D. Westfall *et al.*, *Phys. Rev.* **C19**, 1309 (1979).
- [7] K. Summerer, B. Blank, *Phys. Rev.* **C61**, 034607 (2000).
- [8] J.R. Cummings *et al.*, *Phys. Rev.* **C42**, 2508 (1990).
- [9] B.S. Nilsen *et al.*, *Phys. Rev.* **C52**, 3277 (1995).
- [10] R. Silberberg, C.H. Tsao, *Phys. Rep.* **191**, 351 (1990).

- [11] C.H. Tsao *et al.*, *Phys. Rev.* **C47**, 1257 (1993).
- [12] L. Sihver *et al.*, *Phys. Rev.* **C47**, 1225 (1993).
- [13] J.W. Wilson *et al.*, NUCFRG2: An Evaluation of Semiempirical Nuclear Fragmentation Database, NASA TP-3533 (1995).
- [14] V.E. Dudkin *et al.*, *Nucl. Phys.* **A509**, 783 (1990).
- [15] V.E. Dudkin *et al.*, *Nucl. Phys.* **A568**, 906 (1994).
- [16] W.R. Webber *et al.*, *Phys. Rev.* **C41**, 520 (1990).
- [17] S. Cecchini *et al.*, *Nucl. Phys.* **A807**, 206 (2008).
- [18] C. Zeitlin *et al.*, *Phys. Rev.* **C56**, 388 (1997).
- [19] W.R. Webber, D.A. Brautigam, *Astrophys. J.* **260**, 894 (1982).
- [20] P. Ferrando *et al.*, *Phys. Rev.* **C37**, 1490 (1988).
- [21] W.R. Webber, J.C. Kish, D.A. Schrier, *Phys. Rev.* **C41**, 533 (1990).
- [22] W.R. Webber *et al.*, *Phys. Rev.* **C41**, 547 (1990).
- [23] P. Napolitani *et al.*, *Phys. Rev.* **C70**, 054607 (2004).
- [24] P. Napolitani *et al.*, *Int. J. Mod. Phys.* **E13**, 333 (2004).
- [25] C. Villagrasa-Canton *et al.*, *Phys. Rev.* **C75**, 044603 (2007).
- [26] Yu.E. Titarenko *et al.*, *Phys. Rev.* **C78**, 034615 (2008).
- [27] R.J. Charity *et al.*, *Nucl. Phys.* **A483**, 371 (1988).
- [28] J. Aichelin, *Phys. Rep.* **202**, 233 (1991).
- [29] N. Wang *et al.*, *Phys. Rev.* **C65**, 064608 (2002).
- [30] S. Ota *et al.*, *Radiat. Meas.* **43**, S195 (2008).
- [31] H.L. Bradt, B. Peters, *Phys. Rev.* **77**, 54 (1950).
- [32] G. Iancu *et al.*, *Radiat. Meas.* **39**, 525 (2005).